Hydrodynamic phenomena in laser physics: Modes with flow and vortices behind an obstacle in an optical channel

M. Vaupel, K. Staliunas, and C. O. Weiss
Physikalisch-Technische Bundesanstalt, 38116 Braunschweig, Germany
(Received 16 February 1995; revised manuscript received 20 February 1996)

The transverse patterns of an active resonator with cylindrical optics are investigated. This resonator configuration corresponds to a ''channel'' form of the potential for the ''photon fluid.'' Simultaneous emission of different transverse modes along the channel, periodic nucleation of vortices in the form of a vortex street (vortices of alternating senses of rotation appearing in a flow behind an obstacle), accelerated flow in a ''tilted channel,'' and destabilization of the one-directional flow in the channel are demonstrated and interpreted in terms of tilted waves and beating of channel modes, as well as in fluid terms, illustrating the fluid dynamics correspondence of class-A lasers. [S1050-2947(96)02407-9]

PACS number(s): 42.60.Jf, 42.65.−k, 61.72.Lk

I. INTRODUCTION

We report on the transverse field structures of lasers with cylindrical resonator optics. We use a photorefractive oscillator (PRO) as a class-A-laser model system [1]. For its convenient dynamic time scale this arrangement lends itself particularly to studies of pattern dynamics in active optical systems [2–4]. The cylindrical resonator optics is used to produce predominantly one-dimensional (1D) phenomena. This arrangement, although corresponding to a large-aspect-ratio system, does not allow one to realize pure 1D cases in general: besides the purely 1D patterns (with intensity varying only along one direction), 2D patterns were also observed (with intensity varying also along the other direction). We interpret these quasi-2D patterns as higher-order 1D Hermite modes with internal ''flows'' along the ''channel'' direction.

This arrangement allows us to obtain controllable, directed streams of the ''photon fluid'' and to observe various hydrodynamic analogs in nonlinear optics, like the vortex street behind an obstacle in a flow.

The experimental observation of these predominantly 1D patterns motivated our theoretical study. We give here the general description of photon fluid motion in this channel together with results of numerical simulations. The theoretical model of a PRO with a cylindrical resonator is given in Sec. III. In Sec. IV experimentally observed stationary modes with internal flows of such a resonator are shown and discussed. When one of the resonator mirrors is tilted in the channel direction, modes with accelerating flows are obtained (Sec. IV). Section V gives the case of two Hermite modes, simultaneously emitted at different locations along the channel of equal frequencies, whereas in Sec. VI those modes beat, which can be hydrodynamically interpreted as a von Kármán vortex street. The question of multimode coexistence is also theoretically discussed in the same section. Dark waves traveling along the channel are shown in Sec. VII.

II. EXPERIMENTAL SETUP

We use a ring resonator (perimeter 2 m, Fig. 1) with an even number of mirrors in order not to suppress helical fields [5] which correspond to optical vortices. The oscillator consists of a bismuth silicate (BSO) crystal (length 5 mm, cross section 5×5 mm^2) as the active medium and plane mirrors (one of them movable by a piezo element, and another one tiltable by a piezo element). Two cylindrical lenses ($f=10$ cm, with a distance of ca. 21 cm between them) are used to fix the frequency spacing between neighboring transverse modes belonging to the same longitudinal order to a little more than 3/4 of the free spectral range. This means that the resonator configuration is stable in one direction: nearly concentric with a spacing between adjacent transverse modes belonging to different adjacent longitudinal orders of a little less than one-quarter of a free spectral range. The order of neighboring transverse mode thus increases not towards higher frequencies but towards lower frequencies in this

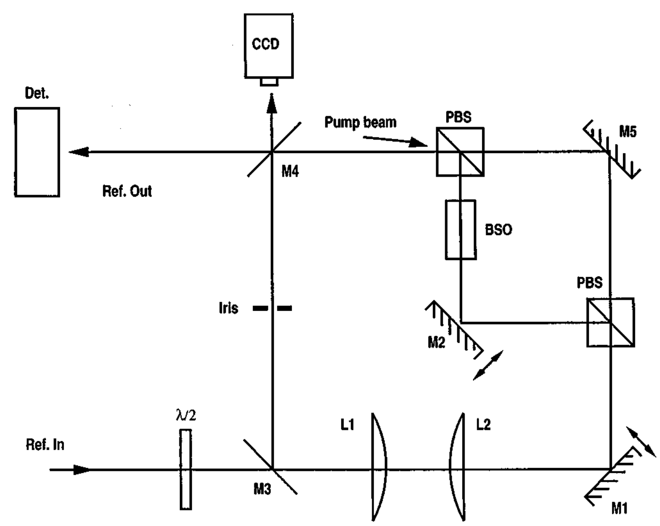

FIG. 1. Experimental setup. The active resonator is formed by four mirrors $M1-M4$ and the active BSO crystal. PBS: polarizing beam splitter. The resonator formed by $M1$, $M3$, $M4$, and $M5$ has high finesse and is used for resonator-length stabilization. The reference signal is provided by part of the pump radiation with polarization perpendicular to pump and generated field traveling oppositely to the generated field.

near-concentric configuration. It is unstable (plane) in the other direction; thus the field is confined in one direction and free to move in the other direction, as in a channel.

Two apertures (rectangular slit and circular iris) limit the excitation of transverse modes. The long side of the slit lies parallel to the focal line of the cylindrical lenses (x direction). To reproducibly excite certain mode families, the resonator length is actively stabilized relative to the pump (=emission) frequency in a fashion described in [5]. The resonator length can be controlled by the movable mirror. A change in length shifts the modes of the resonator with respect to the gain line of the active medium. Thus it is possible to separately excite particular transverse-mode families.

The slit is used to control the losses of the modes in the y direction (perpendicular to the focal line of the cylindrical lenses) so that we select the highest excitable transverse mode by this aperture. Without the iris the optical field is widely extended along the (unstable) x direction. The iris was used to limit the length of the patterns. This was also found to increase the gain near the optical axis.

For optical amplification in the resonator the BSO photorefractive crystal is pumped by a single-frequency Ar^{+} laser (514 nm) whose intensity is around 3 mW/cm^2. The crystal is illuminated uniformly (within 5%). As required for gain a dc field (5 kV) is applied across the crystal, because BSO is a drift-type photorefractive material [6]. 10% of the light generated is coupled out and recorded by a charge-coupled device (CCD) camera.

III. MODEL OF PRO WITH CYLINDRICAL RESONATOR OPTICS

We employ the theoretical model for PRO's discussed in detail in [7,8,4]. The total optical field $E(\vec{r},t)$ in the resonator and the total index of refraction $n(\vec{r},t)$ are written in terms of the slowly varying envelopes: $E(\vec{r},t)=E_p(\vec{r},t)\exp(i\vec{k}_p\cdot\vec{r}-i\omega_p t)+E(\vec{r},t)\exp(i\vec{k}_r\cdot\vec{r}-i\omega_r t)+\text{c.c.}$ and $n(\vec{r},t)=n(\vec{r},t)\exp(i\vec{q}\cdot\vec{r}-i\Omega t)+\text{c.c.}$ Here $E_p(\vec{r},t)$ and $E_r(\vec{r},t)$ are the envelopes of the pump and generated fields respectively, $\Omega=\omega_p-\omega_r$, and $\vec{q}=\vec{k}_p-\vec{k}_r$. Using the mean field (single-longitudinal-mode) approximation and neglecting the depletion of the pump wave leads to the following dynamical equations for drift-type PRO's [1,4]:

$$\frac{\partial E_r}{\partial t}=k[-(1+i\beta_0)E_r+i\Delta\omega_\perp(\vec{\nabla}^2/4-r^2)E_r+iE_p n^*], \tag{1}$$

$$\frac{\partial n}{\partial t}=-\gamma[n-i\Omega n/\gamma-n_s E_p E_r/I_0]. \tag{2}$$

Here $I_0=|E_p(\vec{r})|^2+|E_r(\vec{r})|^2$, κ is the photon decay rate, γ is the relaxation rate of the refractive index grating ($\gamma\ll\kappa$), n_s is the saturated value of the refractive index grating (depending on the applied dc voltage), β_0 is the resonator frequency detuning from the gain line center, $\Delta\omega_\perp$ is the frequency separation of adjacent transverse-mode families of the empty resonator, $\vec{\nabla}^2=(1/r^2)(\partial^2/\partial_\phi^2)+(1/r)(\partial/\partial_r)+\partial^2/\partial_r^2$ is the Laplace operator in the plane normal to the optical axis of the PRO, and $\vec{r}=(r,\phi)$ are the polar coordinates in this plane; the coordinate z is directed along the optical axis of the system.

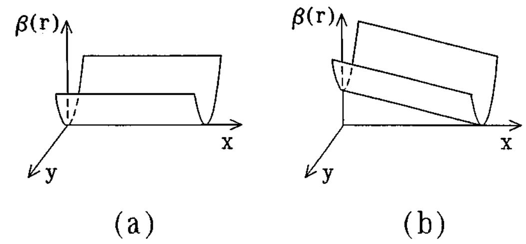

FIG. 2. Hydrodynamic potential $\beta(r)$ for the PRO in a resonator with cylindrical optics (a) without and (b) with tilt of one mirror into the x direction.

The spatial coordinates are normalized to the radius of the fundamental Gaussian (TEM_{00}) mode of the resonator, and the frequencies β_0 and $\Delta\omega_\perp$ in (1) are normalized to the width of the TEM_{00} to empty resonator resonance.

The fast variable of optical field is adiabatically eliminated from the system (1) and (2), which leads to an equation of complex Swift-Hohenberg type [9]:

$$\frac{\partial E}{\partial\tau}=p(1+i)E-i(\beta-d\vec{\nabla}^2)E-(\beta-d\vec{\nabla}^2)^2E/4 -(1+i)E|E|^2. \tag{3}$$

Here $p=(n_s-2)/n_s$ is the pump parameter, $d=\Delta\omega_\perp/4$, $E=E_r/E_p\sqrt{2/n_s}$ is the normalized optical field (order parameter), and $\tau=t\gamma n_s/2$ is the normalized (slow) time. The curvature of the resonator mirrors is taken into account by a spatially dependent detuning parameter $\beta(\vec{r})$. For resonators with spherical mirrors $\beta(\vec{r})=\beta_0(\vec{r})-1+\Delta\omega_\perp r^2$; for resonators with cylindrical mirrors $\beta(\vec{r})=\beta_0(\vec{r})-1+\Delta\omega_\perp y^2$, if the mirrors focus in the y direction.

An equation similar to (3) was also derived for class-A lasers in [9–11]. (3) differs from the class-A-laser amplitude equation in the defocusing term only (the imaginary part of the nonlinear term). Since PROs and class-A-lasers are described by the same amplitude equation (3), one sees the PRO–class A-laser analogy [1]. Consequently, the results reported in this article on pattern formation in PROs are directly applicable also for class-A lasers.

The role of the spatially dependent $\beta(\vec{r})$ can be understood from the hydro-dynamics analogy of nonlinear optics [10]. The Madelung transformation brings (3) to the form of fluid-dynamical equations for the motion of a viscous and quantized photon fluid in a potential of form $\beta(\vec{r})$. In the case of a cylindrical resonator the potential $\beta(\vec{r})$ is of the form of a channel as illustrated by Fig. 2(a). When the resonator mirrors are tilted in the (x,z) plane, the potential tilts as illustrated by Fig. 2(b). In this case the expression for the potential $\beta(\vec{r})$ transforms to $\beta(\vec{r})=\beta_0(\vec{r})-1+\Delta\omega_\perp y^2-\alpha x$, where α is the tilt parameter.

The analysis of the photon flow in the channel is done by using the complex Swift-Hohenberg equation (CSHE) (3). In numerical investigations we integrated the initial PRO equations (1) and (2). [We integrated (1) and (2) on a 256×256 spatial grid using a split-step numerical scheme.)

IV. TRANSVERSE MODES OF CHANNEL ARRANGEMENT

A. Modes in an untilted channel

The simplest stationary solutions of the CSHE (3) in the case of zero tilting (α=0) are

$$E(\vec{r},\tau)=E_n H_n(y)e^{-y^2/2+ik_{n,x}x}. \tag{4}$$

Here $E_n=\sqrt{p}$, $dk_{n,x}^2=1-\beta_0-(n+1/2)\Delta\omega_\perp$, and H_n is the nth-order Hermite polynomial. The expression (4) describes a Gauss-Hermite mode transverse to the channel with a phase gradient $\vec{\nabla}\phi=\vec{k}_{n,x}$ directed along the channel.

The physical meaning of the excitation of channel modes can be understood in the following way. The modulus of the total wave vector of the radiation is determined by the radiation frequency, $|\vec{k}|=w_0/c$. The total wave vector can be decomposed into spatial components:

$$\vec{k}^2=k_{n,x}^2+k_y^2+k_z^2. \tag{5}$$

The longitudinal z component of $\vec{k}$ is fixed due to the longitudinal-mode selection. In the case when only one channel mode is excited, the y component of $\vec{k}$ is also fixed. Then the x component of $\vec{k}$ (along the channel) is $k_{n,x}^2=\vec{k}^2-k_y^2-k_z^2$. This means that $k_{x,n}$, and consequently the angle of $\vec{k}$ with respect to the optical axis, depend on the detuning β_0. The angle increases with increasing negative detuning. Further increase of negative detuning leads to excitation of the next higher-order transverse mode of the channel.

The gradient of the field phase along the channel $\vec{\nabla}\phi=(k_{n,x},0)$ corresponds to a flow along the mode. Indeed, the Madelung transformation [13] leads to the following relation between the gradient of the phase, and the velocity of flow: $\vec{v}=2d\vec{\nabla}\phi=2d\vec{k}_{n,x}$. In the PRO case this means that every local (along x) perturbation of a mode moves with the velocity $\vec{v}=2d\vec{k}_{n,x}$ along the channel [see also Eq. (7) below]. This can be seen by rewriting (3) in terms of x-dependent channel modes $f_n(x,\tau)$:

$$\frac{\partial f_n}{\partial\tau}-2dk_{n,x}\frac{\partial f_n}{\partial x}=p(1+i)f_n+id\frac{\partial^2 f_n}{\partial x^2}+d^2k_{n,x}^2\frac{\partial^2 f_n}{\partial x^2}-(1+i)\Gamma|f_n|^2 f_n. \tag{6}$$

Here $\Gamma=\int_{-\infty}^{\infty}H_n^4(y)\exp(-2y^2)dy$, and $E(\vec{r},\tau)=f_n(x,\tau)H_n(y)\exp(-y^2+ik_{n,x}x)$.

Every longitudinal modulation of this channel mode in the first approximation moves along the channel axis, as determined by the left-hand side (LHS) terms of (6). Due to the RHS terms of (6) the perturbation is additionally affected by diffusion, diffraction, and nonlinear saturation during the propagation. However, in the leading order the perturbation moves along the channel with constant velocity $v=2dk_{n,x}$. This is why we call (4) modes with flow (or tilted modes).

The mode tuning curve is given in Fig. 3(a), which summarizes the above. The tuning curve in Fig. 3(a) is valid for a single-longitudinal-mode PRO. However, the tuning curve for experiments differs from that in Fig. 3(a). A near-concentric configuration was used in the experiments. As a consequence, the neighboring higher-order transverse mode is located not to the right [as in Fig. 3(a)] but to the left. This changes the mode tuning diagram significantly [see Fig. 3(c)].

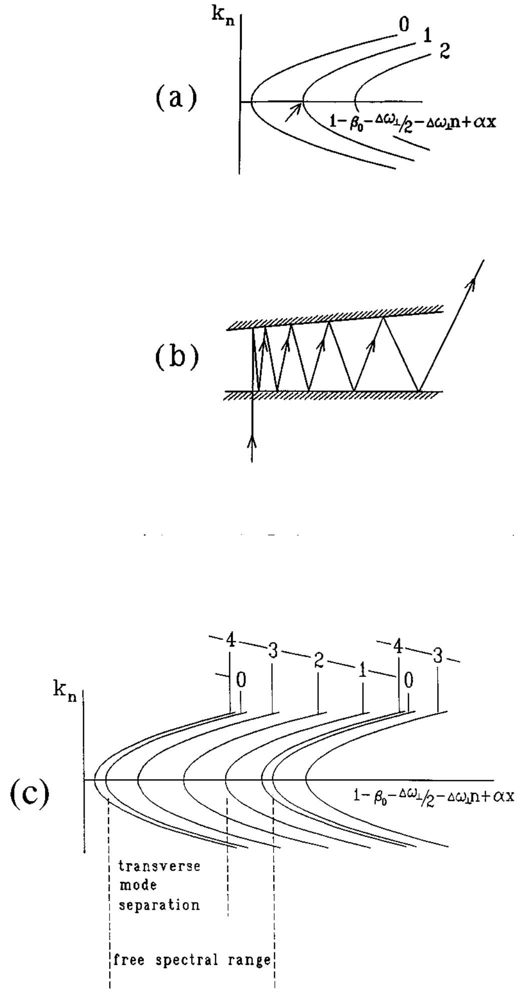

FIG. 3. (a) Solutions of the linearized version of (3) in the form of modes with accelerating flow (the indices indicate the transverse order of modes with flow). The plot may be considered also as the mode tuning curve for the zero-tilt case (α=0). (b) An illustration of acceleration of flow in geometrical optics. (c) The tuning diagram [analog of (a)] for the resonator configuration used in the experiments (the near-concentric case).

The pure modes with flow exist only in an infinitely long channel. In the case of a finite length of the channel the traveling waves reflect from the ends of the channel, resulting in standing waves. The standing wave–traveling wave competition depends on the spatial size (the length of the channel) as investigated in [9]. Following the analysis of [9] it can be expected that in a relatively short channel a standing wave along x will be excited, while in a long but finite channel the traveling wave dominates, but with nonzero standing-wave components (source and sink) at the channel ends. Thus, in general, the resulting field is

$$E(\vec{r},t)=H_n(y)e^{-y^2}[f_{n+}(x)e^{ik_{n,x}x}+f_{n-}(x)e^{-ik_{n,x}x}]. \tag{7}$$

This shows ‘‘ripples’’ along the mode with flow. The presence of ripples allows one to measure the velocity of the flow in the mode.

B. Modes in a tilted channel

The case of nonzero tilt of the channel ($\alpha \neq 0$) can modify the modes in two aspects: (1) the flow within the mode accelerates along the x direction and (2) two different transverse modes with flows can be simultaneously excited in the channel.

Acceleration can be understood from geometrical optics: the angle of a light ray with respect to the optical axis increases on each reflection from the tilted mirror, as illustrated in Fig. 3(b). The solution of Eq. (6) in the leading order also yields modes with accelerating flow:

$$dk_{n,x}^2 = 1 - \beta_0 - \Delta\omega_\perp(1/2 - n) + \alpha x, \tag{8}$$

which is plotted in Fig. 3(a).

The acceleration in a tilted channel can also be interpreted by considering that the resonator length is now a function of the x coordinate. Consequently, k_z and $k_{x,n}^2$ are also functions of x:

$$k_z(x,\alpha') = \frac{2\pi q}{L - \alpha' x} \simeq \frac{2\pi q}{L}(1 + \alpha' x/L). \tag{9}$$

Here L is the resonator length and q is the longitudinal-mode number. (9) is inserted into (5), where k and k_y are x independent. The result is

$$k_x^2(x,\alpha') = k^2 - k_y^2 - \left(\frac{2\pi q}{L}\right)^2 - \frac{8(\pi q)^2}{L^3}\alpha' x. \tag{10}$$

This leads to the same expression (8). The relation of the actual tilting angle α (and the normalized one, α) can be obtained by comparing (8) and (10).

Similarly to the case of zero tilt, two counterpropagating traveling waves are excited for a channel of finite length. One of the traveling waves travels uphill and the other downhill in the channel. This results again in a standing wave with nonequidistant nodes (dark vertical stripes). The distance between nodes is inversely proportional to the local flow velocity.

C. Experimental observations

In the experiment a narrow slit along the x axis was used in order to increase the losses of higher-order transverse modes (in the y direction), which allows us to excite only one mode with flow. Figure 4(a) shows the stationary pattern of the zero-order mode emitted from a resonator with one tilted mirror. The presence of the ripples allows the measurement of flow velocity. The velocity increases from left to right in Fig. 4(a). The velocity was determined by measuring the distances between adjacent nodes and bright maxima of intensity of Fig. 4(a), and is given in Fig. 4(b), which confirms the $k_x^2 \simeq x$ proportionality, with the slope proportional to the tilt angle α.

A series of recordings similar to Fig. 4 but with different tilt angles is shown in Fig. 5, where Fig. 5(a) is recorded without tilt. The bright spot marks the optical axis. Each one of the following figures 5(b)–5(d) was recorded with a larger tilt angle than the figure before it. The patterns show the above vertical dark stripes whose mutual distances decrease with the distance from the optical axis, corresponding to increasing flow velocity. They also show that the maximum of the intensity is shifted away from the optical axis with increasing tilt angle.

D. Numerical results

We calculated numerically modes with flow and modes with accelerating flow in the channel configuration of the PRO. The integration for a tilted channel of finite length yields ‘‘downhill’’ as well as ‘‘uphill’’ flow (Fig. 6). For small values of tilt α, bistability between uphill and downhill modes with flow was observed [in the limiting case of zero tilt ($\alpha=0$) the bistability of left and right traveling modes is evident, because of symmetry considerations]. With increasing tilt, only the downhill wave remains. The ripples in Fig. 6 indicate the remnants of the mode with opposite flow, which appear due to reflection from the boundaries at the ends of the channel. The flow velocities within the fundamental H_0 mode are plotted in Fig. 7 for different values of tilt. With small deviations near the two ends of the channel the relationship fits satisfactorily with the square-root dependence (8).

V. TWO MODES IN THE CHANNEL

The previous section deals with relatively small tilts of the channel. This causes acceleration of flow in a single mode. Larger angles of tilt lead to simultaneous excitation of two different channel modes with flows. This situation is schematically shown in Fig. 8, where TEM_{00} and the first transverse mode TEM_{01} are simultaneously excited. The simultaneous excitation can be interpreted by considering that the tilt of the channel results in different lengths of the resonator along the channel and thus different resonance conditions. If the difference of resonator length corresponds to the frequency separation between transverse modes, then the simultaneous excitation of neighboring transverse modes is possible.

A corresponding experimentally recorded pattern (the second- and third-order modes with flow emitted simultaneously) is shown in Fig. 9.

For investigation of this multimode case, Eq. (3) is rewritten in mode decomposition: $E(\vec{r},\tau)\ \Sigma_{n=o}^{\infty} f_n(x,\tau)A_n(y)\exp(ik_{n,x}x)$, where $A_n(y)$ are envelopes of Hermite modes. Differently from the usual mode expansion, the coefficients f_n are functions not only of time τ, but also of coordinate x. Equation (3) for the nontilted channel transforms to

$$\frac{\partial f_n}{\partial \tau} - 2dk_{n,x}\frac{\partial f_n}{\partial x} = p(1+i)f_n + id\frac{\partial^2 f_n}{\partial x^2} + d^2k_{n,x}^2\frac{\partial^2 f_n}{\partial x^2}$$
$$-(1+i)\sum_{klm=0}^{\infty}\Gamma_{klmn}f_kf_lf_m^*. \tag{11}$$

Here $\Gamma_{klmn} = \int_{-\infty}^{\infty}A_kA_lA_m^*A_n^*dy$ are the transverse-mode cross- and auto-correlation coefficients. (11) is a 1D system of coupled complex Ginzburg-Landau equations.

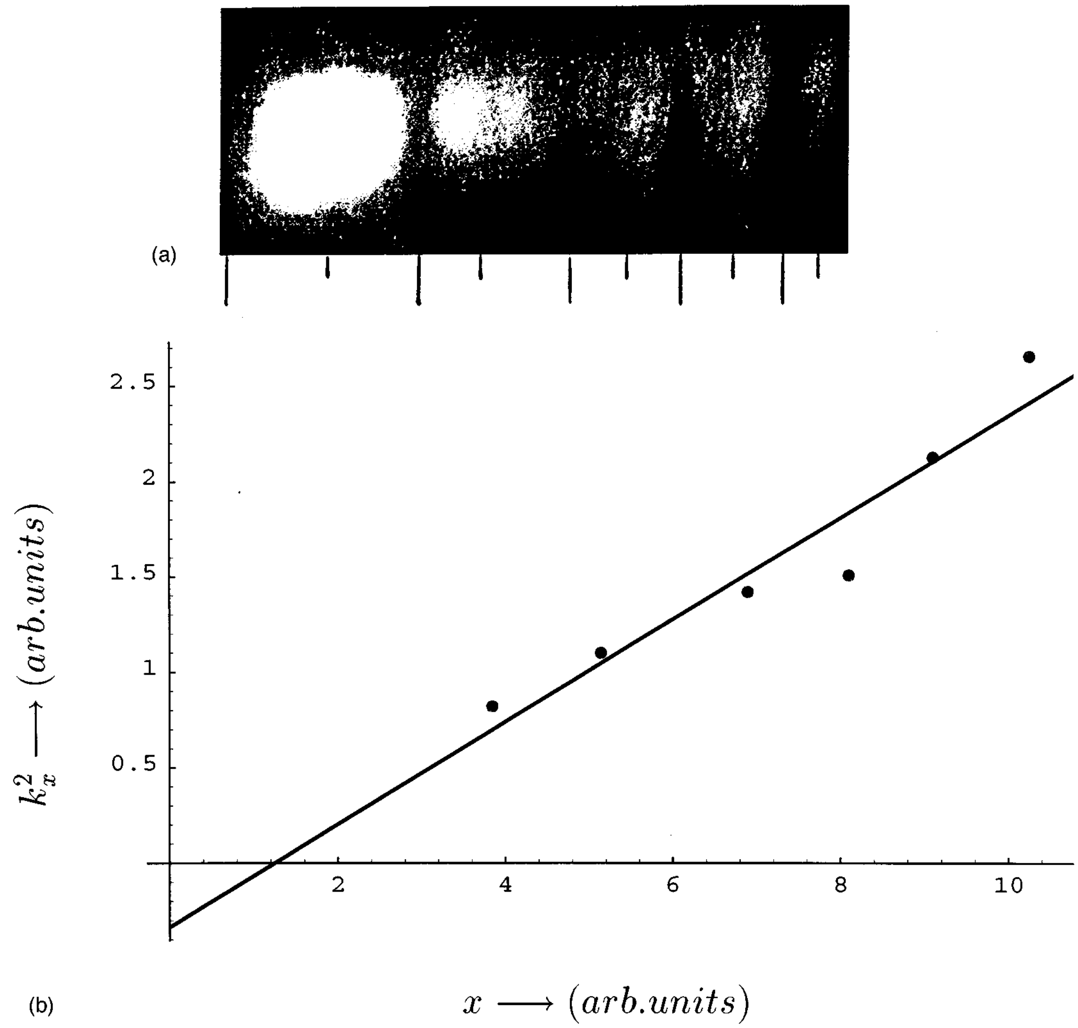

FIG. 4. (a) Pattern of the fundamental mode in a resonator with a slightly tilted mirror. Minima and maxima of intensity marked. (b) k_x^2 as a function of x measured from (a), indicating an accelerated flow.

In the case of only two transverse modes, the properties of solutions of (11) depend mainly on the values of cross correlation coefficients between the two modes. The modes compete if the normalized cross correlation of the modes is large: $G_{ij}=\Gamma_{iijj}/\sqrt{\Gamma_{iiii}}\sqrt{\Gamma_{jjjj}}>\frac{1}{2}$, and coexist if $G_{ij}<\frac{1}{2}$ (see also [14]). We calculated (Table I) the cross-correlation coefficients G_{ij} of the first ten modes. As seen, neighboring modes with flows never do coexist.

This is in accordance with the experimental observations, showing that two different modes with flows are always well separated along the x axis and have only a small zone of overlap along the x axis as Fig. 9 illustrates. The interference pattern of two modes without flow is plotted in Fig. 10 as calculated by approximating the mode overlap by a tanh function:

$$A_0(x,y)=\tfrac{1}{2}[1+\tanh(-x)]H_0(y)e^{-y^2}, \quad H_0(y)=1, \tag{12}$$

$$A_1(x,y)=\tfrac{1}{2}[1+\tanh(x)]H_1(y)e^{-y^2}, \quad H_1(y)=y. \tag{13}$$

Figure 10 shows the merging of black stripes in the overlap region between two transverse modes at three different phase differences. Depending on the actual phase difference between the two modes the black stripe of the H_1 mode can end in the center between these modes [Fig. 10(b)] or continue towards the left mode upward or downward [Figs. 10(a) and 10(c)].

VI. NONSTATIONARY CHANNEL PATTERNS

If the different transverse modes are of different frequencies, nonstationary patterns occur. To illustrate such dynamics in the case of two modes with flow we multiply the mode amplitudes from (12) and (13) by phase factors $e^{ik_{0,x}x-i\omega_1\tau}$ and $e^{ik_{1,x}x-i\omega_2\tau}$. In this case, vortices (phase singularities of the field) appear in the overlap zone. Figures 11(a) and 11(b) and show snapshots during a beat period calculated for an interference pattern of the zero- and the first-order transverse modes. Both figures [11(a) and 11(b)] show the following from right to left. A straight dark stripe of the first-order mode deforms into a wavy line whose amplitude increases towards the zero-order mode. The stripe breaks up into vortices near the zero-order mode. The wavelength of the wavy dark line and the distance between two neighboring vortices depend on the relative flow velocity of the modes, which is proportional to $k_{2,x}-k_{1,x}$.

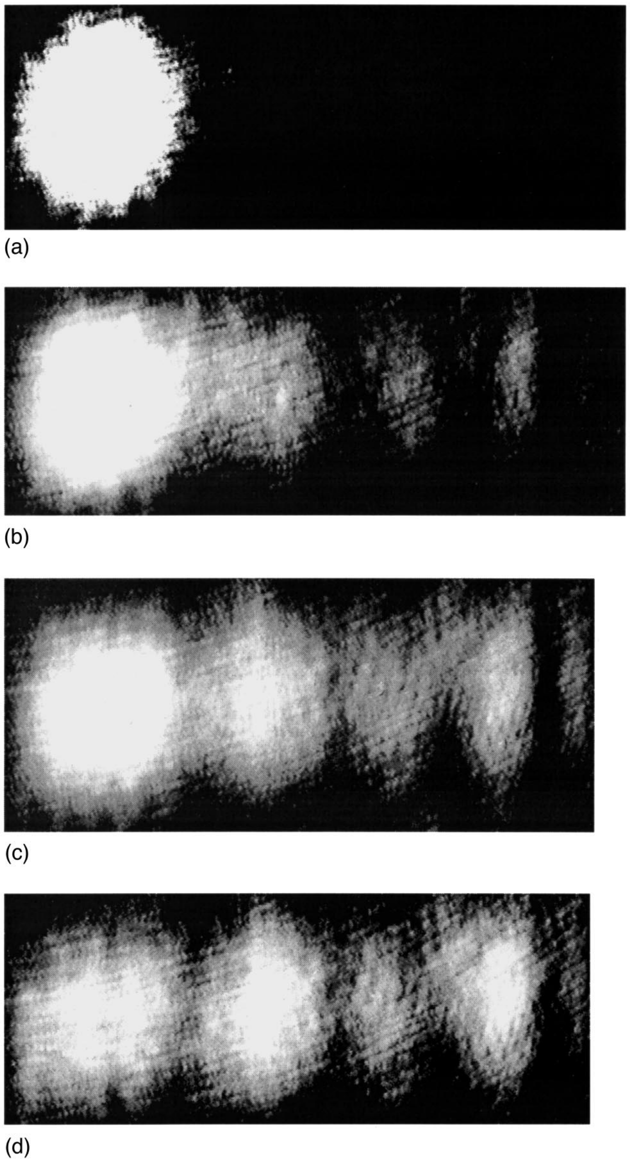

FIG. 5. (a) Pattern like Fig. 4(a) but without mirror tilt. (b) –(d): The same as in (a) but with increasing tilt angle from (b) to (d). α_b=0.7, α_c=1.4, α_d=2.2 (arbitrary units).

Motion of the wavy dark line and periodic generation of vortices occur if the overlapping modes have different frequencies ω_0 and ω_1. Then the pattern moves essentially along the x direction corresponding to the difference frequency between the modes. The vortices in addition are moving outward in the y direction. The vortices generated alternate in topological charge. Positively charged vortices move upward, negatively charged ones downward.

A. Vortex street

The periodic nucleation of vortices described is shown experimentally in two snapshots [Figs. 12(a) and 12(b)] for the case of fundamental and first-order mode emitted. In this case the mode overlap in space is much larger than in the pattern of Fig. 9. The vortices (marked by rectangles) move away from the wavy black stripe on the right, alternately to either the upper or lower part of the left side of the picture.

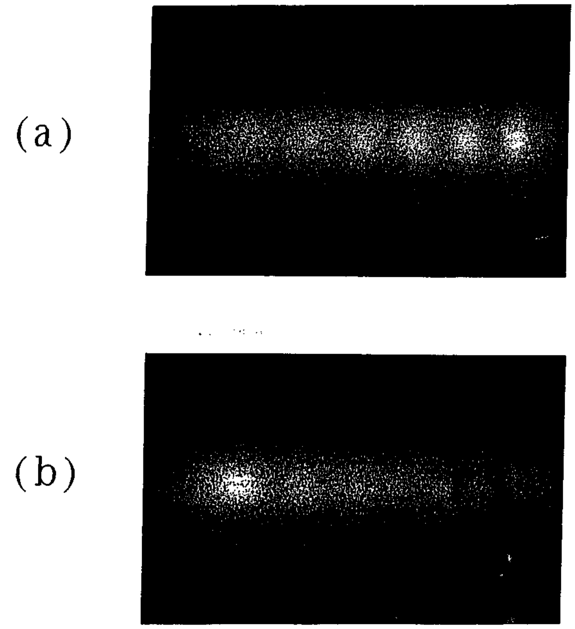

FIG. 6. Modes with downhill (a) and uphill (b) flow in the channel of finite length (l_{chann}=8, the spatial coordinate is normalized to the width of the fundamental Gaussian channel mode), as obtained by numerical integration of (1) and (2). A slit parallel to x was introduced to restrict the generation to the fundamental mode H_0 of width d_y=1.75. The mode with flow into the opposite direction to the dominating one is also present. This results in the ripples along the mode. Parameters are α=0.075, n_s=4 (p=0.5), γ=0.01, $\Delta\omega_\perp$=1, and β_0=−0.75.

The frequency with which vortices move through a fixed point on the vortex trajectory, corresponding to the beat frequency of the two modes, is shown as measured as a function of resonator mirror tilt angle in Fig. 13. Near a particular tilt angle α_0 it is possible to completely stop the motion of the vortices, which implies phase locking of the two modes. For angles smaller (larger) than α_0 the direction of vortex

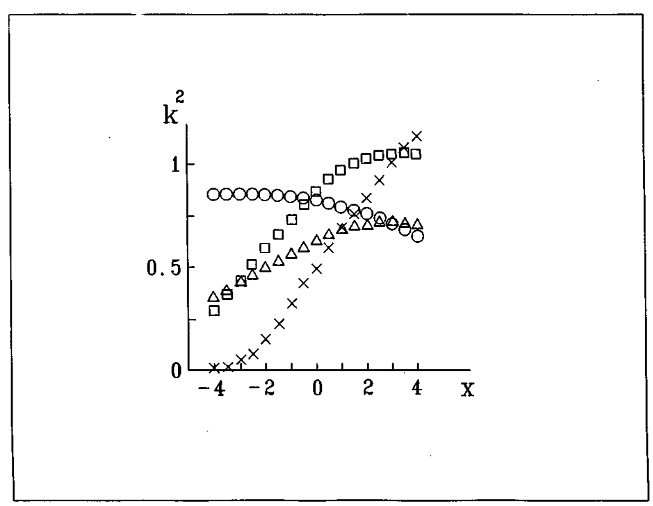

FIG. 7. The variation of the flow velocity along the H_0 mode for different tilts α. The parameters are as in Fig. 6 (except for tilts α). Circles are for zero tilt α=0, triangles, α=0.1, squares, α=0.2, and crosses, α=0.3.

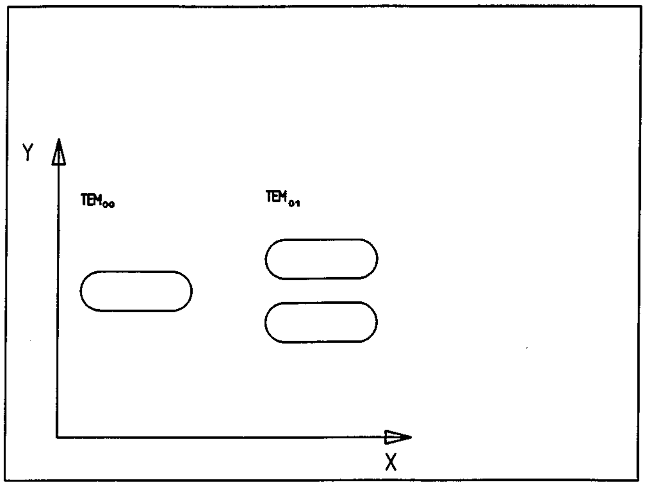

FIG. 8. Fundamental and first transverse modes emitted from a tilted channel resonator.

motion is to the right (left). The angle α_0 does not correspond to an untilted resonator. Frequency pulling of modes by the gain line determines the beat frequency.

Figure 14 shows the intensity measured at two locations on the upper trajectory as a function of time while the resonator mirror tilting is reduced. The phase difference between the signals before and after the transition through α_0 (marked by A) clearly shows the reversal of direction of the vortex motion.

Figure 15 shows a snapshot series of the field corresponding to Figs. 12(a) and 12(b) using interference with part of the pump beam [15]. These interferograms represent a positively charged vortex as a fork in the interference fringes which opens upward and a negatively charged vortex at a fork opening downward. As apparent, consecutively generated vortices alternate in topological charge.

We find it remarkable that this optical analog of vortex creation behind an obstacle in a flow (vortex street) can be realized with only two modes. The ''obstacle'' here is represented by the dark line of the Hermite 01 mode. Here the photon density is zero as at the location of a real obstacle in a flow. This dynamic vortex street of an active lasing resonator reminds us of the static one in a diffraction pattern behind a needle [12].

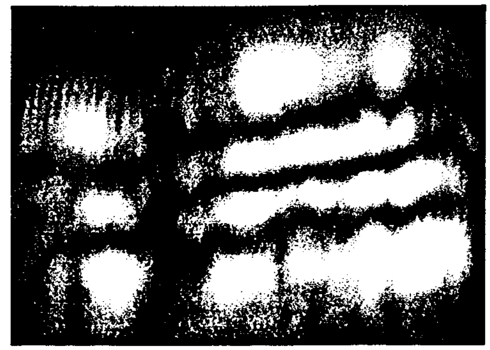

FIG. 9. PRO emission pattern consisting of the second- (left) and third- (right) order one-dimensional transverse modes.

To stress the similarity with the hydrodynamic vortex street further, the velocity-field corresponding to Fig. 12(a) obtained by the Madelung transformation [13] of the optical field is shown in Fig. 12(c). Vortices are marked by dots.

The ingredients of this experimental realization of vortex obstacle flow in a laser are as follows.

(1) Two modes are emitted spatially separated but with some spatial overlap.

(2) The waves corresponding to these modes are tilted with respect to the optical axis by different amounts (different flow velocities in the modes). This creates the vortices as a result of three-beam interference [16]. The observation of vortices here is thus a definite experimental proof of the existence of tilted waves [17] in lasers.

(3) The modes have different optical frequencies. This results in the dynamics of the flow. It is conceivable that the different frequencies and the different tilts of the modes result in the following way. One mode is detuned negatively and consequently tilted and not frequency pulled. The other mode is detuned positively (untilted wave fronts are parallel to the mirrors, and consequently frequency pulled). In a plane resonator with one tilted mirror the modes—in addition to tilt—have the freedom to adjust their positions laterally (in order to adjust their emission frequency to the center of the gain line); thus it is not completely evident in detail how the relative tilt and frequency difference comes about (probably due to nonlinear interaction of the two active

TABLE I. Normalized cross-correlation coefficients of the first ten Hermite modes (from $n=0$ to 9): $G_{ij}=\Gamma_{iijj}/\sqrt{\Gamma_{iiii}}\sqrt{\Gamma_{jjjj}}$.

	0	1	2	3	4	5	6	7	8	9
0	1.0	0.577	0.468	0.412	0.376	0.350	0.330	0.314	0.301	0.290
1	0.577	1.0	0.631	0.523	0.465	0.427	0.399	0.377	0.360	0.345
2	0.468	0.631	1.0	0.656	0.552	0.494	0.455	0.426	0.404	0.386
3	0.412	0.523	0.656	1.0	0.673	0.571	0.513	0.474	0.445	0.423
4	0.376	0.465	0.552	0.673	1.0	0.684	0.585	0.528	0.489	0.460
5	0.350	0.427	0.494	0.571	0.684	1.0	0.693	0.595	0.539	0.501
6	0.330	0.399	0.455	0.513	0.585	0.693	1.0	0.700	0.604	0.548
7	0.314	0.377	0.426	0.474	0.528	0.595	0.700	1.0	0.706	0.611
8	0.301	0.360	0.404	0.445	0.489	0.539	0.604	0.706	1.0	0.711
9	0.290	0.345	0.386	0.423	0.460	0.501	0.548	0.611	0.711	1.0

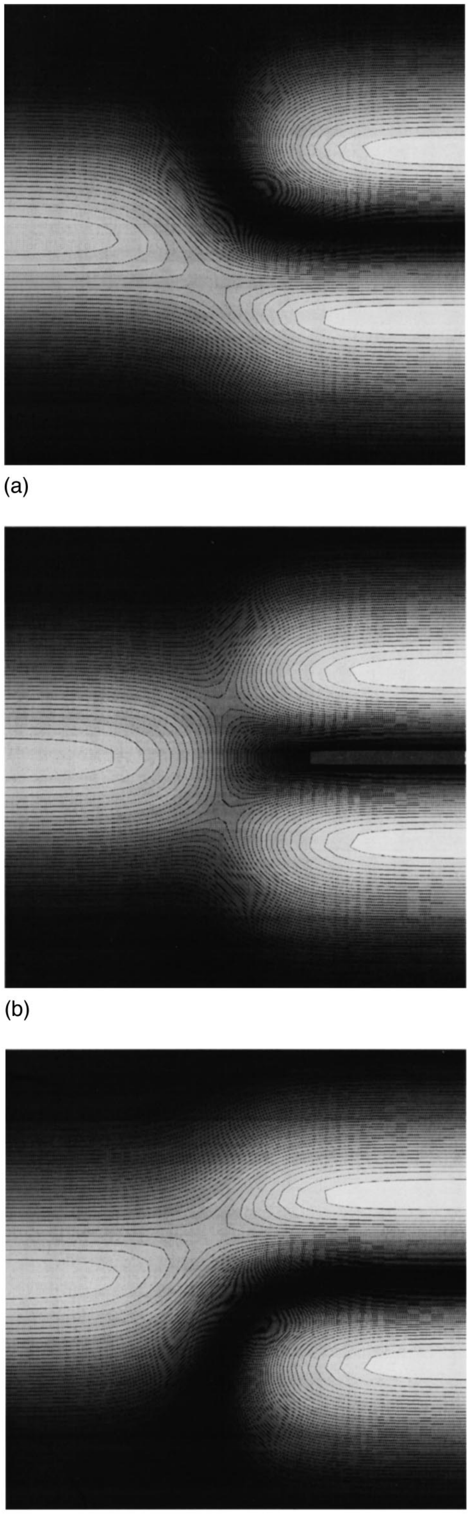

(a)
(b)
(c)

FIG. 10. (a) Calculated intensity pattern in the overlap region between zero- (left) and first- (right) order transverse modes. The two modes have the same frequency and tilt. (b) and (c): The same as in (a) but each taken one-quarter of the beat period after the preceding panel.

modes). The observed dynamics, and in particular the appearance of vortices, in any case shows that a difference between the two modes in tilt and optical frequency exists in the experiment.

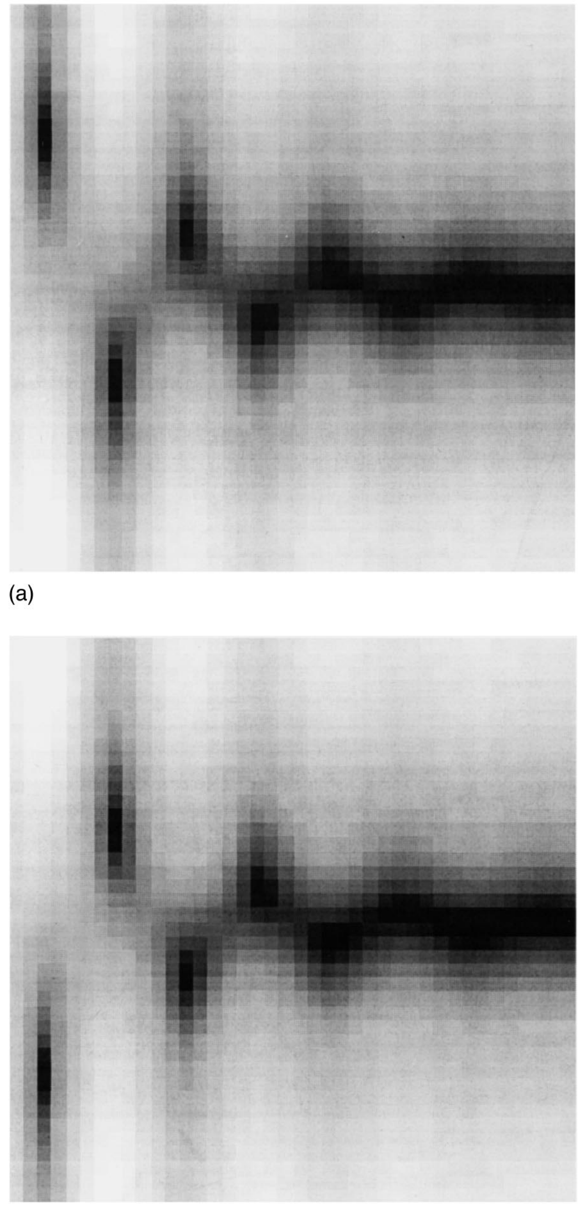

(a)
(b)

FIG. 11. (a) Pattern calculated for the modes of Fig. 10(a) but with nonzero mutual velocity (tilt). (b) The same taken one-half of a beat period later.

B. Lateral destabilization of flow

If two modes cross-correlate weakly, $G_{ij}<\frac{1}{2}$, then they can be excited simultaneously in the whole length of the channel, as follows from (11). In the single-longitudinal-mode case such a situation is impossible, since all neighboring transverse modes overlap too much (Table I) and compete. However, using different longitudinal-mode families such a situation can be realized. As seen from Fig. 3 the configuration used in the experiments allows one to make the modes TEM_{00} and TEM_{04} coincide in optical frequency. These two modes overlap weakly, and as follows from Table I can coexist along the whole channel.

Corresponding recordings in Fig. 16 give a series of snapshots with a slightly tilted mirror. The motion shown can be explained by the beating between the fundamental mode and

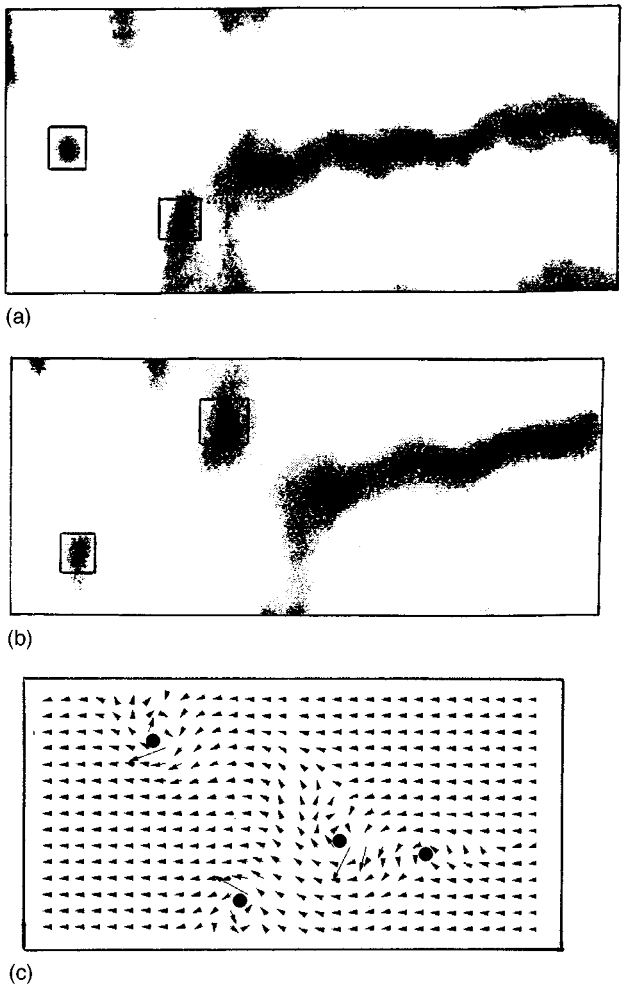

FIG. 12. (a) and (b): Snapshots of the vortex creation in the overlap region between fundamental and first-order transverse modes. The wavy black line on the right splits into vortices (marked by rectangles) moving to the left (experimental). (c) Velocity field corresponding to Fig. 11(a), calculated by means of the Madelung transformation. Vortices marked by dots.

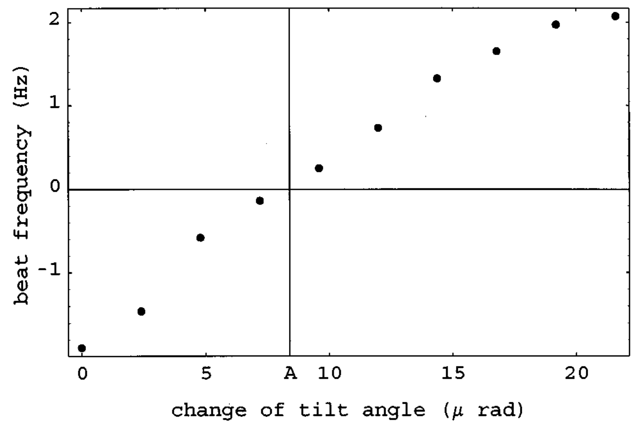

FIG. 13. Frequency of vortex nucleation in Figs. 12(a) and 12(b) as function of tilt angle of one resonator mirror. At tilt A ($\cong\alpha_0$) the motion of vortices goes to zero, indicating mode locking.

a weak fourth-order transverse mode whose frequency is close to the frequency of the fundamental mode in this particular resonator and whose center is beyond the left edge of the pictures. The pattern shown is similar to a wave moving to the left on a rope with a fixed right end. This pattern corresponds to the destabilization of a one-dimensional channel flow in the transverse direction.

The amplitude of the fourth-order mode beating with the fundamental mode increases towards the left end of the picture, but it is still smaller there than the amplitude of the fundamental mode. The right end of the fundamental mode stays time independently at its y position, because at this end the field of the fourth-order mode is negligibly small.

Vertical dark stripes in the picture indicate again the existence of two waves, a right traveling wave and a left traveling wave of the fundamental mode (see Sec. IV), which interfere.

A pattern similar to Fig. 16, resulting from beating between zero- and first-order transverse modes is shown in Fig. 17. A dark vertical interference stripe divides the picture. The stripe is a part of a standing-wave pattern as explained in Sec. IV. This pattern is similar to a Hermite mode $H_{1,1}$. Although there is no focusing along the x direction, the finite aperture of the resonator (Fresnel number=5–10) lifts the transverse-mode (along the x direction) frequency degeneracy. Only a plane resonator of infinite Fresnel number would have modes degenerate in frequency. Hermite modes H_{n_x,m_y} induced by the aperture were observed up to the ninth order (i.e., $H_{9,0}$). The transverse-mode spacing between such neighboring modes was then 10% of the free spectral range.

On the right-hand side of Fig. 17 the intensity contour is essentially straight, as the amplitude of the second (interfering) mode is very small. The upper and lower edges of the pattern on the left side resemble a sinusoidal wave which is traveling to the left. The upper and lower edges of the pattern are deformed here in the same way as the dark central stripe. The motion of the profile and the wavy shape on the left side of the picture are due to (1) the fundamental-mode amplitude increasing towards the left, although it is everywhere much smaller than the amplitude of the first-order mode, and (2) the difference in tilt between the first- and zero-order mode.

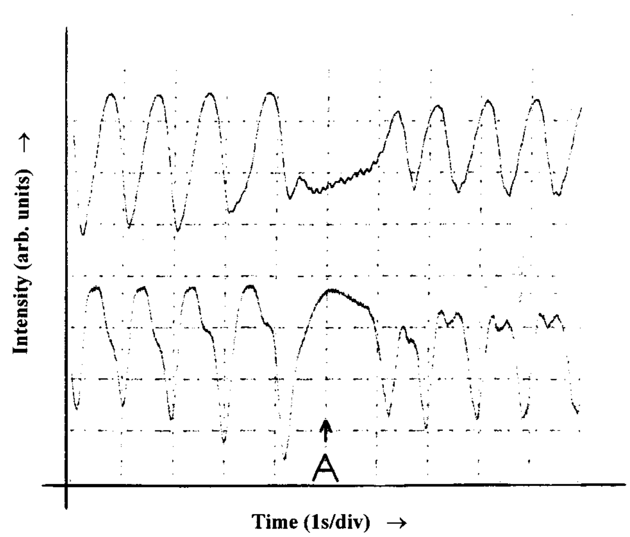

FIG. 14. Intensity measured at two points on the vortex trajectories of Fig. 12(a) while changing the tilt of one resonator mirror. At tilt A ($\cong\alpha_0$) the direction of motion of the vortices reverses.

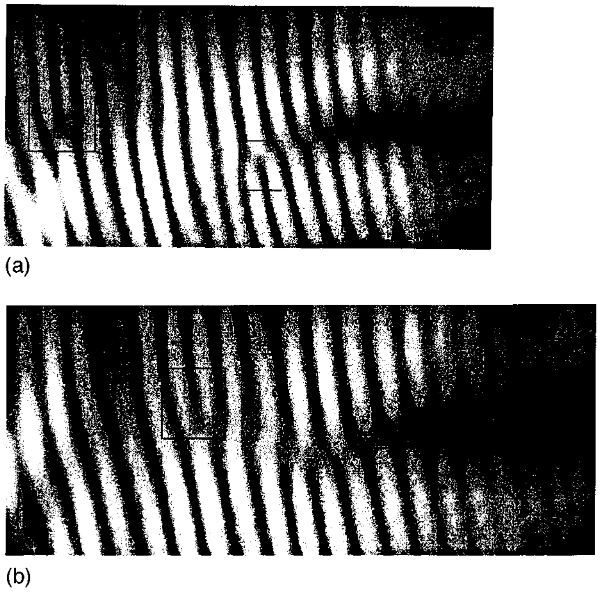

FIG. 15. (a) and (b): Interferograms corresponding to Fig. 12(a). The ''forks'' correspond to a vortex. Direction of fork gives the sign of the topological charge of the vortices. (a) and (b) are taken at different times.

We could not reproduce numerically the dynamics observed experimentally (the series of snapshots in Figs. 16 and 17) which show the lateral destabilization of the fundamental mode with flow along the stream. The lateral destabilization in Figs. 16 and 17 is different from that predicted theoretically (Figs. 14 and 15) and from what one may expect from the hydrodynamical analogy. This difference follows from the peculiarities of the tuning curve of our resonator: as seen from Fig. 3(c) the fundamental H_0 mode is very close in frequency to the H_4 mode, which results in a beat between these two modes. We note that such a situation never occurs in hydrodynamics, nor in the numerical integration of PRO equations (1) and (2), where the modes H_0 and H_4 are never neighboring ones in the single-longitudinal-mode approximation.

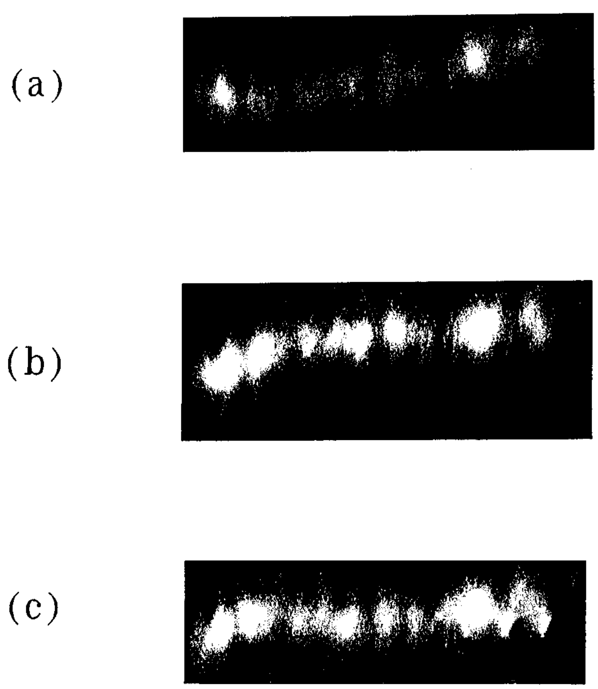

FIG. 16. Snapshots of patterns of a wave of large wavelength traveling along the fundamental mode.

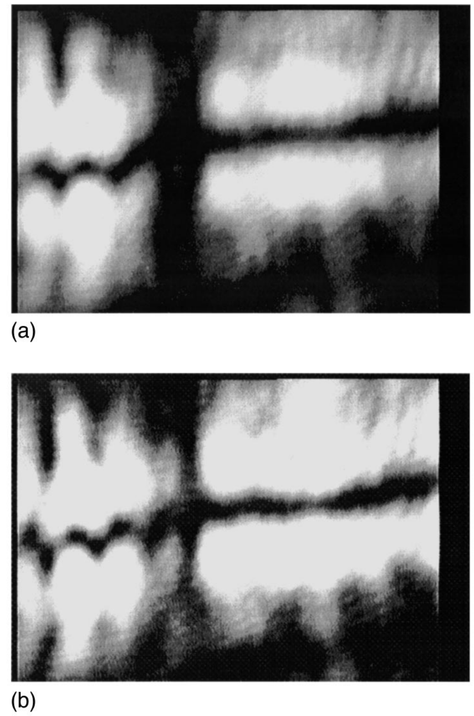

FIG. 17. Snapshots of patterns of a wave traveling along the first-order transverse mode with large amplitude on the left side and small amplitude on the right side. The pattern is due to the simultaneous emission of the fundamental mode (outside the picture on the left). In (b) the wave has traveled the distance of one-half of one wavelength with respect to (a).

C. Numerical results

Solutions containing modes from two neighboring mode families may exist if modes with left and right flow directions are considered. Linear stability analysis of (11) shows that the resonantly tuned mode $H_1(1-\beta_0-3/2\Delta\omega_\perp=0\Rightarrow k_{1,x}=0)$ is unstable with respect to simultaneous excitation of the left and right flowing H_0 modes. This means that instead of a pure resonantly tuned H_1 mode, the ''dressed'' H_1' mode is emitted:

$$E(x,y,\tau)=A_0(y)[f_0^+\ \exp(ik_0x)+f_0^-\ \exp(-ik_0x)]\pm if_1A_1(y). \tag{14}$$

Here $|f_0^+|=|f_0^-|^2=p/(3\Gamma_{0000})$ and $|f_1|^2=p/\Gamma_{1111}$. Such a numerically calculated dressed H_1' mode is shown in Fig. 18, and contains vortices with alternating topological charge.

The dressed H_1' mode is stationary, since time dependence is absent in (14). The value of detuning corresponding to the stationary H_1' mode is marked in Fig. 3(a) by an arrow.

When the resonator is tuned towards the higher transverse modes (to the right from the arrow, $1-\beta_0-3/2\Delta\omega_\perp$

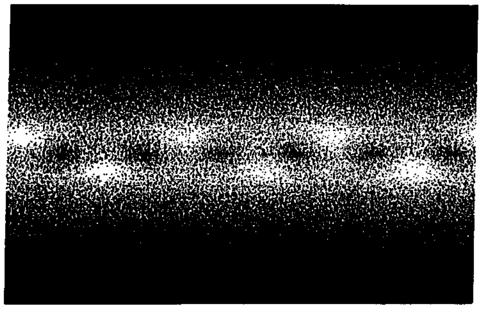

FIG. 18. Stationary dressed H_1' mode (Gaussian+first-order transverse mode) in an infinitely long channel as obtained from the numerical integration of (1) and (2) with periodic boundaries along x. Parameters are $n_s=4$ ($p=0.5$), $\gamma=0.01$, $\Delta\omega_\perp=1$, $\beta_0=-0.5$, and the length of the integration region along x is $l_{\rm chann}=10$. Negative detuning $\beta_0<-0.5$ results in translational motion of the intensity distribution along the channel.

$>0\Rightarrow k_{1,x}\neq 0$) the dressed mode (similar to the pure mode with flow) starts to move. The three-mode solution of (11) takes the following form:

$$E(x,y,\tau)=A_0(y)\{f_0^+\exp[i(k_0+k_1)x-i\omega\tau] + f_0^-\exp[-i(k_0+k_1)x-i\omega\tau]\} \pm if_1A_1(y)\exp(ik_1x). \quad (15)$$

Inserting (15) into (11) one obtains $dk_1^2=1-\beta_0-3/2\Delta\omega_\perp$ [coinciding with (8) for the pure mode with flow], $dk_0^2=\Delta\omega_\perp$, $\omega=2dk_0k_1$, and the mode coefficients f_n coincide with those for stationary dressed modes (14). The (phase and group) velocity of propagation of the dressed mode along the channel is $v=\omega/k_0=2dk_1$ and thus equals that of the pure mode with flow. Since the intensity of the dressed mode is modulated along the x axis (e.g., Fig. 18), the intensity pattern also moves then as a traveling dressed mode, differently from the pure mode with flow, where only the nonzero phase gradient k_x indicates the flow in the mode.

The motion of dressed modes occurs when one (or two) participating pure modes are off resonance. For the detunings towards the higher-order transverse modes [to the right of the arrow in Fig. 3(a)] the H_0 modes are off resonance, and thus they are frequency pulled [see (15)]. This results in a translational motion of the dressed mode. For detunings towards the lower-order modes, the H_1 mode is off resonance. This results in an oscillatory motion of the dressed mode (not yet investigated in detail).

Increase of negative detuning leads to emission of dressed modes of higher order. As seen from Fig. 3(a), if the nth-order mode is emitted, then all modes of order from 0 to n may also be emitted. All of these modes (of order from 0 to n) result in an nth-order dressed mode H_n, which travels with the velocity of the pure nth-order mode with flow [8].

Coexistence of only two modes from the neighboring mode families may occur when the channel is not perfectly parallel. Due to imperfections in the channel (linear) coupling between the modes occurs, violating the mode coexistence condition given above ($G_{ij}<\frac{1}{2}$). Figure 19 shows the result of the integration of the PRO equations (1) and (2) for a channel with widening. In the wider region of the channel

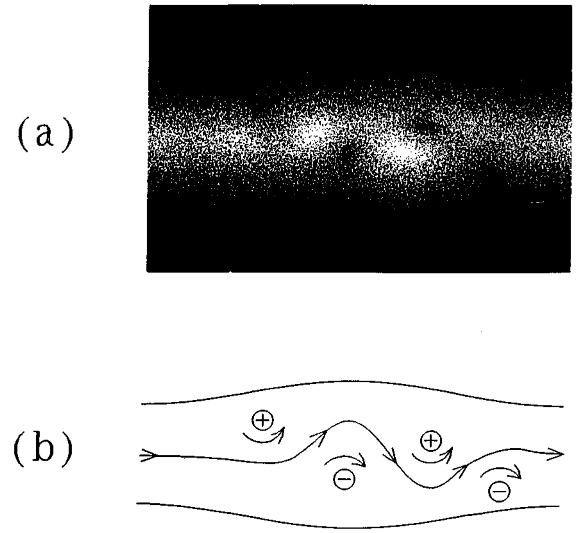

FIG. 19. Transverse instability of the stream and formation of vortices in the widening of the channel as obtained from the numerical integration of (1) and (2) with periodic boundaries along x. Parameters are $n_s=4$ ($p=0.5$), $\gamma=0.01$, $\beta_0=-0.30$, and $\Delta\omega_\perp=1$ (the inverse width of the channel), which is a function of x: $\Delta\omega_\perp=1=1-0.25\cos(2\pi x/l_{\rm chann})$.

the initially parallel stream of the photon fluid destabilizes, and this leads to the appearance of optical vortices in the widened part of the channel. This means that in the narrow part of the channel the pure fundamental mode H_0 is emitted, and in the wide part the dressed mode H_1' is excited.

Finally, a tilted channel of finite length was numerically investigated. Conditions were as in Fig. 6, except for the detuning β_0: the detuning was chosen such that the fundamental mode H_0 was emitted in the left part, and the mode

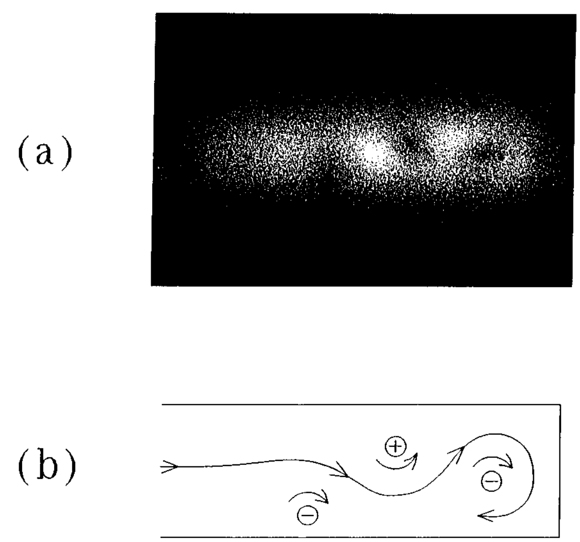

FIG. 20. Transverse instability of the stream and formation of vortices in the tilted channel of finite length, as obtained from the numerical integration of (1) and (2). Parameters are as in Fig. 6, except for a slit. The slit was absent, which allowed excitation of the higher-order modes and thus the transverse instabilities of the photon flow.

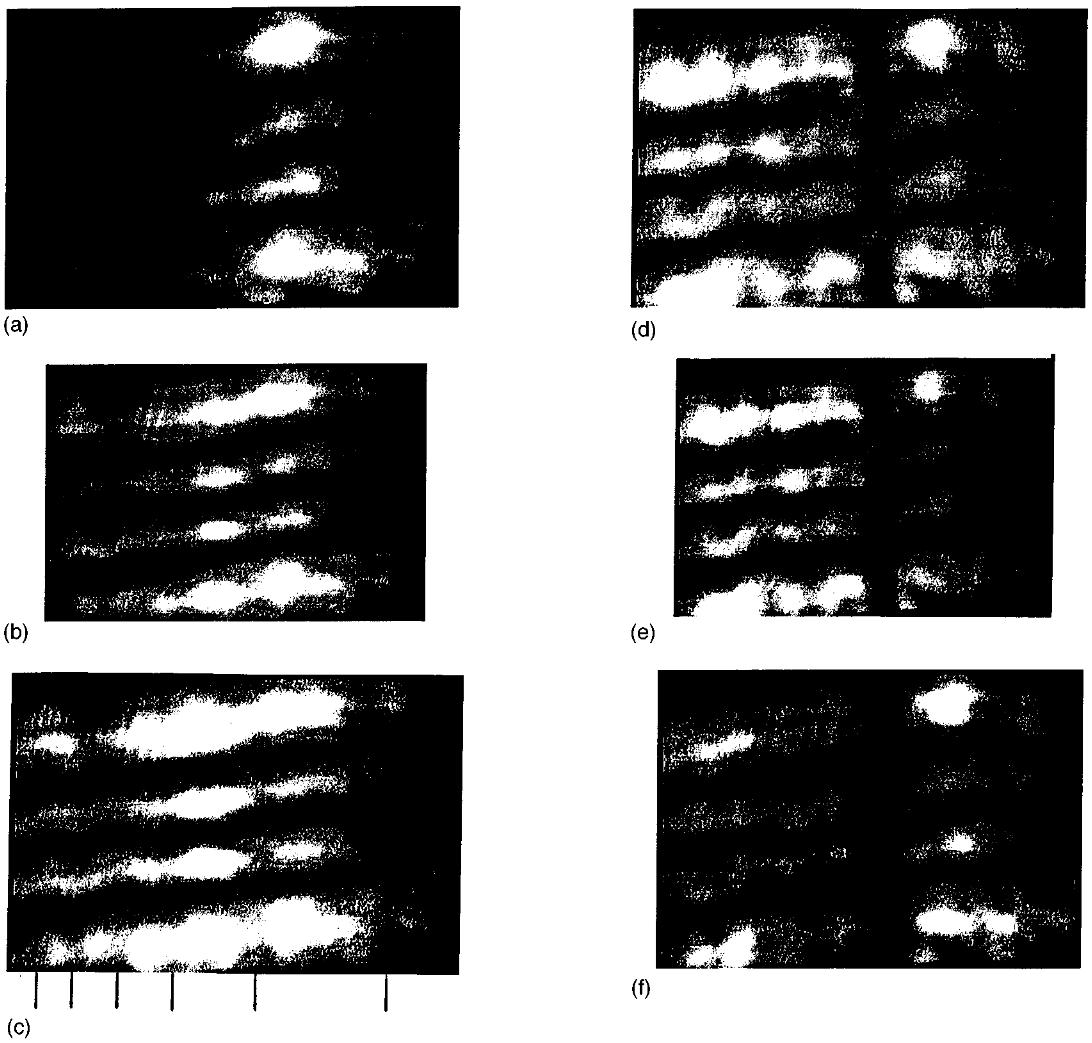

FIG. 21. Snapshots of the third-order transverse mode with flow from the right to the left periodic in time. A dark structure moves periodically from right to left. The dark vertical stripe and the other stationary vertical stripes of smaller contrast indicate a standing wave due to simultaneous emission of the wave with opposite tilt. For details, see the text.

H_1' in the right part of the channel. As seen from Fig. 20 the photon fluid accelerates along the tilted channel, until it destabilizes and breaks into optical vortices.

VII. TRAVELING WAVES

As follows from [9] perturbations travel along the x direction with the velocity $2dk$. Such behavior is typical for systems dominated by traveling waves [18,19]. The spatial perturbations (dark solitons, vortices) move with the mean flow of the traveling waves.

As follows from (6) (see also [9]) the x- and t-dependent part of such solutions can be described with a spatially traveling envelope $a(x-vt)$ by

$$A(x,t)=A_0a(x-vt)e^{ik_xx}e^{-i\omega t} \tag{16}$$

with $v=2dk_x$. Such periodically horizontally moving patterns of the kind (16) were experimentally observed with all transverse modes. Figure 21 uses the third-order mode as an experimental example. It is a series of snapshots within one period in which the motion is periodic. As can be seen, an intensity minimum moves to the left. The intensity maximum reaches the left end of the picture in Fig. 21(e). At this time the right part of the mode has the lowest intensity. After this the intensity drops in the left part and the intensity of the right part rises again to a maximum. This evolution repeats periodically. Some vertical dark stationary stripes [Fig. 21(d)] similar to the stripes in Fig. 4 can be seen as an intensity modulation. These stripes indicate an acceleration of the flow to the left obeying (10).

A periodic motion of a dark stripe similar to Fig. 21 was recently shown for a similar case of a photorefractive oscillator with spherical mirrors [20]. In this case the moving pattern arose from the zero- and first-order Hermite modes with a periodic modulation of the amplitudes caused by nonlinear mode interaction. The traveling dark wave of Fig. 21 can be interpreted similarly.

It could otherwise also be a dark solitary wave as found in our numerical integrations of (3). We give one realization of such a pattern in Fig. 22. There appear dips (the ‘‘dark soli-

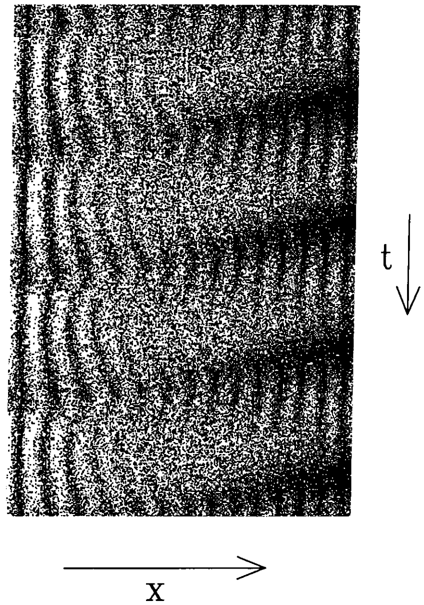

FIG. 22. Periodic dynamics of the flow along the untilted channel as obtained by numerical integration of (3). Parameters are $p=1.5$ and $\beta_0=-1.5$; the other parameters are as in Fig. 6. The coordinate along the channel is the horizontal one; time is the vertical coordinate and changes over $\Delta t=120$ from top to bottom.

tary waves'') of the field at one end of the channel, which move together with the flow. The velocity of the dark solitary waves corresponds to the flow velocity, as the numerical investigations show.

VIII. CONCLUSION

Optical flow phenomena have been demonstrated on a photorefractive oscillator which is equivalent to a class-*A* laser near threshold. The observed patterns can be interpreted in a mode picture or alternatively in a hydrodynamics analogy. The effect of tilting one resonator mirror on the beat between two adjacent modes in space and the optical spectrum, on the relative velocity between these transverse modes, and on the pattern formation in the overlap region was investigated. Periodic vortex creation in the overlap region between modes constitutes an example of real vortex flow in an optical system of the kind of ''vortex creation behind an obstacle.'' Transverse destabilization of one-dimensional flow is found in the case of different field amplitudes of spatially separated modes.

Dark waves traveling in a single mode show agreement with solutions of the complex Swift-Hohenberg equation for the PRO and for class-*A* lasers, for which stationary and periodic solitary patterns were found. Those solitary waves can be described by standing waves with a traveling envelope.

ACKNOWLEDGMENTS

This work was supported by Deutsche Forschungsgemeinschaft under Grant No. We743-9/1 and E. O. Goebel Leipnitzpreis. M. Vaupel acknowledges financial support from the Friedrich Naumann Stiftung.

[1] K. Staliunas, M. F. H. Tarroja, G. Slekys, and C. O. Weiss, Phys. Rev. A **51**, 4140 (1995).
[2] D. Hennequin, L. Dambly, D. Dangoisse, and P. Glorieux, J. Phys. (France) III **4**, 2459 (1994).
[3] F. T. Arecchi, S. Boccaletti, P. L. Ramazza, and S. Residori, Phys. Rev. Lett. **70**, 2277 (1993).
[4] G. D'Alessandro, Phys. Rev. A **46**, 2791 (1992).
[5] M. Vaupel and C. O. Weiss, Phys. Rev. A **51**, 4078 (1995).
[6] P. Yeh, *Introduction to Photorefractive Nonlinear Optics* (Wiley, New York, 1993).
[7] N. V. Kukhtarev, V. B. Markov, S. G. Odulov, M. S. Soskin, and V. L. Vinetskii, Ferroelectrics **22**, 940 (1979).
[8] D. Z. Anderson and R. Saxena, J. Opt. Soc. Am. B **4**, 164 (1987).
[9] K. Staliunas and C. O. Weiss, Physica D **81**, 79 (1995).
[10] K. Staliunas, Phys. Rev. A **48**, 1573 (1993).
[11] J. Lega, J. V. Moloney, and A. Newell, Phys. Rev. Lett. **73**, 2978 (1994).
[12] G. A. Swartzlander, Jr., and C. T. Law, Phys. Rev. Lett. **69**, 2503 (1992).
[13] E. Madelung, Z. Phys. **40**, 322 (1926).
[14] K. Staliunas, M. F. H. Tarroja, and C. O. Weiss, Opt. Commun. **102**, 69 (1993).
[15] More detail about the interferometric visualization of vortices can be found in A. G. White *et al.*, J. Mod. Opt. **38**, 2531 (1991).
[16] M. Berry, in *Physics of Defects*, edited by R. Balian (North-Holland, Amsterdam, 1981).
[17] P. K. Jakobsen, J. V. Moloney, A. C. Newell, and R. Indik, Phys. Rev. A **45**, 8129 (1992).
[18] G. K. Harkness, W. Firth, J. B. Geddes, J. V. Moloney, and E. M. Wright, Phys. Rev. A **50**, 4310 (1994).
[19] L. Gil, Nonlinearity, **4**, 1213 (1991).
[20] B. M. Jost and B. E. A. Saleh, Phys. Rev. A **51**, 1539 (1995).